An Intermediate Model for Fitting Triplet-Triplet Annihilation in Phosphorescent Organic Light Emitting Diode Materials.

Paul Niyonkuru,[1] Andrew P. Proudian,[1] Matthew B. Jaskot,[2] and Jeramy D. Zimmerman[1, 2, *]

[1] *Department of Physics, Colorado School of Mines, Golden, CO 80401, USA*
[2] *Materials Science Program, Colorado School of Mines, Golden, CO 80401, USA*

Triplet-triplet annihilation (TTA) is one of the primary contributors to efficiency roll-off and permanent material degradation in phosphorescent organic light-emitting diodes (OLEDs). The two limiting case models typically used to quantify this quenching mechanism are multi-step Dexter and single-step Förster, which respectively assume ideal Fickian diffusion or perfect trapping of triplet excitons. For device-relevant guest doping levels (typically 5-12 *vol*%), both significant diffusion of excitons and trapping due to spatial and energetic disorder exist, so neither conventional model fits experimental data well. We develop and validate an intermediate TTA model, which is a weighted average of the limiting cases of pure radiative decay (no TTA) and multi-step Dexter based TTA that returns an effective TTA rate constant and a parameter quantifying the portion of well-isolated excitons. Kinetic Monte-Carlo simulations and time-resolved photoluminescence measurements of an archetype host-guest system demonstrate that our intermediate model provides significantly improved fits with more realistic physical values, is more robust to variations in experimental conditions, and provides an analysis framework for the effects of trapping on TTA .

I. INTRODUCTION

Phosphorescent organic light-emitting diodes (OLEDs) are a commercial technology with applications in displays and lighting, yet questions remain about fundamental processes occuring within the materials. Triplet-triplet annihilation (TTA) and triplet-polaron quenching (TPQ) reduce the efficiency of these devices and are thought to be the primary intrinsic mechanisms through which these OLEDs degrade under operational conditions [1, 2]. Models and experiments used to explore these mechanisms should accurately represent the processes occurring and fitting should be robust enough to reveal differences as a device structure is changed without extreme sensitivity to changes in other fit parameters.

Of interest to this paper, TTA occurs when two excitons aggregate onto a single molecule via,

$$T_1 + T_1 = \begin{cases} S_0 + S_n \\ S_0 + T_n, \end{cases} \tag{1}$$

where T_1 is a triplet, S_0 is the ground state, and a highly excited triplet state (T_n with spin = 1) is created roughly 75% of the time, and a highly excited singlet state (S_n with spin = 0) is created in the remaining 25% of cases. While also possible, it is generally energetically unfavorable to generate a quintet (spin = 2)[3–5]. TTA has two primary consequences: first, the efficiency of the device is reduced by the non-radiative elimination of triplets, and second, the S_n or T_n states can have excited state energies in excess of bond enthalpies, which can result in breaking of chemical bonds and irreversible material degradation[6–8].

TTA rates can be extracted by exciting the sample with a short laser pulse of sufficiently high intensity and monitoring the time-resolved photoluminescence (TRPL) decay. The TRPL response is typically fit to one of two limiting cases of the TTA governing equation (*inf.* Equation 2): The multi-step Dexter (MSD, *inf.* Equation 6) model assumes that the excitons are highly mobile and can diffuse readily and eventually aggregate via a Dexter hopping mechanism and annihilate[9, 10]. MSD is, however, only strictly valid in a flat energy landscape where diffusion is truly Fickian. The opposite limit, single-step Förster (SSF, *inf.* Equation 11), is strictly true for the case of fully trapped triplets (no diffusion); here, the excitons are immobile and TTA occurs when two triplets are sufficiently close that exciton aggregation can occur when the energy of one triplet can transfer to another existing triplet via Förster resonant energy transfer (FRET)[10]. The SSF model is appropriate for a well-dispersed emissive guest doped into a host matrix at a low concentration (*e.g.*, less than 1 *vol*%) with large triplet confinement energy $\Delta E_{\mathrm{T}} \equiv E_{\mathrm{T,h}} - E_{\mathrm{T,g}}$, with $E_{\mathrm{T,h(g)}}$ the triplet energy on the host and guest molecules, respectively[11].

When considering the appropriate model for TTA, it is important to consider two key points: First, there is always energy disorder in the frontier orbital energy levels in organic semiconducting materials, which results in partial trapping of excitons. Second, application relevant OLED devices typically have doping levels of 5-12 vol% guest, which will results in some guest molecules being well isolated, yet many percolating pathways exist that allow for exciton diffusion[11–13].

In OLED materials, it is generally thought that exciton diffusion is dominated by Dexter-based transfer[14, 15] while the exciton aggregation step in TTA typically occurs via long-range FRET, resulting in a behavior between the MSD and SSF limiting cases. Indeed, kinetic Monte-Carlo (kMC) simulation-based modeling has shown that the TTA process in physical materials is best

* jdzimmer@mines.edu

replicated when both multistep diffusion and Förster capture are allowed to occur [11, 16, 17]. In their work based on kMC simulations[16, 18, 19], Eersel *et al.* and Zhang *et al.* develop a method of disentangling the relative contributions of MSD and SSF to TTA based on a ratio of two effective rate coefficients $k_{TT,1}$ and $k_{TT,2}$ obtained from a combination of TRPL and photoluminescence quantum yield (PLQY) data. Ligthart *et al.*[11] and Coehoorn *et al.*[17] build on this method to model the effects of exciton confinement and diffusion with the help of KMC simulations assuming randomly distributed emitter dopants. Though useful, the above analyses rely on KMC simulations and the knowledge of quantities such as photoluminescence quantum yield (η_{PL}) and Förster radius ($R_{\mathrm{F,TT}}$) which, in case of experiments, require additional and complex experiments to evaluate and quantities that are not well known, and does not provide information on trapping of excitons due to energetic and spatial disorder.

We, herein propose an intermediate fitting model to TRPL data that does not require additional PLQY measurements or knowledge of Förster radius, provides direct information regarding the influence of exciton trapping, reduces fit residuals, improves fitting stability, and can provide additional insight into the physical mechanism responsible for TTA.

II. THEORY

II.1. Modeling TTA

The triplet exciton population is commonly modeled with a rate equation where triplet's population numbers (n) are reduced in time (t) through a radiative decay with a lifetime (τ) and through a TTA mechanism that occurs at a rate proportional to the square of the number of triplets and a rate coefficient (k_{TT}):

$$\frac{dn}{dt} = -\frac{n}{\tau} - f k_{\mathrm{TT}} n^2, \tag{2}$$

In this case, f is typically set to 1/2, as each TTA event eliminates one of the two excitons involved. In the case of mobile excitons with an isotropic diffusion coefficient D and an exciton localization length of R_L, the continuity equation leads to a TTA rate coefficient k_{TT}[20, 21] of

$$k_{\mathrm{TT}} = 4\pi D R_L \left(1 + \frac{R_L}{\sqrt{\pi D t}}\right). \tag{3}$$

Assuming a time-independent diffusion coefficient D, a general solution to Equation 2 can be obtained [21],

$$\frac{n(t)}{n_0} = \frac{\mathrm{e}^{-t/\tau}}{1 + c\left[\frac{\sqrt{2D\tau}}{R_L}\left(1 - \mathrm{e}^{-t/\tau}\right) + \mathrm{erf}\left(\sqrt{\frac{t}{\tau}}\right)\right]}, \tag{4}$$

with $c = 4\pi n_0 R_L^2 \sqrt{\frac{D\tau}{2}}$. But as shown in Figure 1b, for non-homogeneous systems, spatial and energetic disorder results in a D that is a function of time, with differing diffusion coefficient for short and long time regimes, which limits the usefulness of this solution. In most cases, Equation 2 is solved by approximating the k_{TT} rate in Equation 3 in one of two time regimes, as follows.

II.2. Multi-step diffusion model

In the long-time (high diffusivity) regime, $\frac{R_L}{\sqrt{\pi D t}} \ll 1$, the annihilation rate is approximated to a time-independent rate coefficient

$$k_{\mathrm{TT,h}} \approx 4\pi D_h R_L, \tag{5}$$

resulting in a solution to the rate equation (Equation 2) of

$$\frac{n(t)}{n_0} = \frac{1}{\left(1 + \frac{1}{2} n_0 k_{\mathrm{TT,h}} \tau\right) \exp(\frac{t}{\tau}) - \frac{1}{2} n_0 k_{\mathrm{TT,h}} \tau}. \tag{6}$$

Again, this is the most commonly used equation by experimentalists to fit TRPL data and is typically referred to as the multi-step Dexter (MSD) model.

The rate equation can also be solved in the short-time (low-diffusivity) regime, $\frac{R_L}{\sqrt{\pi D t}} \gg 1$, resulting in an approximated time-dependent rate

$$k_{\mathrm{TT},\ell} \approx 4\sqrt{\pi D_\ell}\, {R_L}^2 t^{-\frac{1}{2}} = k'_{\mathrm{TT},\ell} t^{-\frac{1}{2}}. \tag{7}$$

This limit has generally been dismissed as it would only be relevant at exceedingly short time frames for systems with Fickian diffusion ($\sim 10^{-12}$ s), but is included here for completeness. The solution to the rate equation (Equation 2) in the short-time (low diffusivity limit) regime, using this time-dependent value of k_{TT} is

$$\frac{n(t)}{n_0} = \frac{\exp(\frac{-t}{\tau})}{1 + \left(\frac{1}{2} n_0 k'_{TT,\ell} \sqrt{\pi}\sqrt{\tau}\right) \mathrm{erf}(\sqrt{\frac{t}{\tau}})}. \tag{8}$$

II.3. Single-Step FRET model

The other mechanism by which excitons can move is FRET. The small spectral overlap integral between phosphorescent emission and absorption from the ground state suggests that the Förster contribution to diffusion is negligible[10, 22]. However, a significant spectral overlap between phosphorescent emission and absorption onto a triplet state enables triplet aggregation and single-step Förster(SSF) based TTA to occur[23]. FRET theory, assuming fully trapped triplets, predicts a time-dependent TTA rate of [24]

$$k_{TT,F} = \frac{2\pi^{\frac{3}{2}}}{3} \frac{R_0^3}{\sqrt{\tau t}} = k'_{TT,F} t^{-\frac{1}{2}}, \tag{9}$$

where the Förster radius, R_0, is a function of the spectra overlap integral,

$$R_0^6 = \frac{9000(\ln 10)\kappa^2\Phi_{\mathrm{PL}}}{128\pi^5 \mathrm{N} n^4}\int F_{\mathrm{D}}(\lambda)\sigma_{\mathrm{A}}(\lambda)\lambda^4 \,\mathrm{d}\lambda. \quad (10)$$

Here Φ_{PL} is photoluminescence quantum yield; $0 \leq \kappa^2 \leq 4$ is dipole-dipole orientation factor; and n is the refractive index. The integral J over wavelength λ quantifies the spectral overlap between the area-normalized PL spectrum of donor $F_{\mathrm{D}}(\lambda)$ and the absorption spectrum of acceptor expressed in terms of absorption cross-section $\sigma_{\mathrm{A}}(\lambda)$.

In the SSF case, the solution to the rate equation (Equation 2) is

$$\frac{n(t)}{n_0} = \frac{\exp(-\frac{t}{\tau})}{1 + \left(\frac{1}{2}n_0 k'_{TT,F}\sqrt{\pi}\sqrt{\tau}\right)\mathrm{erf}(\sqrt{\frac{t}{\tau}})}. \quad (11)$$

Note that Equation 8 and Equation 11 have nearly identical form; the difference being the physical origin of the respective k'_{TT}–i.e., the triplet localization length (R_L) or the Förster radius (R_0).

II.4. Intermediate approximation

Working OLED devices are typically doped with between 5 *vol*% and 12 *vol*% of emitting guest molecule in a wide-gap host and energetic site disorder exists amongst guests. Therefore, in a random dispersion, some guests will be well isolated and some exist within percolating pathways; furthermore, there is likely some degree of clustering of the guest species[1].

If one assumes that Dexter-based diffusion processes dominate, that some level of trapping occurs, and that TTA can be explained with Dexter-based mechanism[14], the true TTA behavior lies somewhere between the limits assumed in Equations 6 and 8. Solving Equation 2 between these limits is not analytically tractable since the exact time dependence of D in Equation 3 is not typically known; however, a first-order approximation is to linearly combine the solutions at the limits, by applying a weighting parameter r to Equation 8 and $(1-r)$ to Equation 6, *i.e.*,

$$\frac{n(t)}{n_0} = \frac{r\exp(-\frac{t}{\tau})}{1 + \left(\frac{1}{2}n_0 k'_{TT,\ell}\sqrt{\pi}\sqrt{\tau}\right)\mathrm{erf}(\sqrt{\frac{t}{\tau}})} + \frac{(1-r)}{\left(1+\frac{1}{2}n_0 k_{\mathrm{TT,h}}\tau\right)\exp(\frac{t}{\tau}) - \frac{1}{2}n_0 k_{\mathrm{TT,h}}\tau}. \quad (12)$$

As D_ℓ is small for the population of trapped excitons and they are well localized (*i.e.*, small R_ℓ), we further simplify this by setting $D_\ell^{1/2}R_L^2 \approx 0$, which leads to a negligible triplet interaction rate, $k'_{TT,\ell} = 0$ and

$$\frac{n(t)}{n_0} = r\exp(-\frac{t}{\tau}) + \frac{(1-r)}{\left(1+\frac{1}{2}n_0 k_{\mathrm{TT,h}}\tau\right)\exp(\frac{t}{\tau}) - \frac{1}{2}n_0 k_{\mathrm{TT,h}}\tau}. \quad (13)$$

This equation effectively treats the excitons as two separate populations–one that is trapped in-place and undergoes purely radiative recombination (hence the variable name r) and a second that can diffuse before potentially participating in TTA.

An effective rate coefficient, $k_{TT,eff}$, can similarly be written as a weighted average of respective rate coefficients, i.e.,

$$k_{TT,eff} = rk'_{TT,\ell} + (1-r)k_{TT,h} \approx (1-r)k_{TT,h}. \quad (14)$$

An equation similar to 12 can be formulated using the MSD limit of Equation 6 and the SSF limit of Equation 11. In this case, the SSF rate, $k'_{TT,F}$, would be approximated to zero by taking the limit of a negligibly small Förster radius, which returns equations identical to Equation 13 and Equation 14.

Our intermediate development ignores the physical mechanism responsible for TTA and returns an effective MSD-based k_{TT} in the presence of partial trapping. Due to their equivalent form, it is impossible to differentiate between the mechanisms leading to Equation 8 and Equation 11 from a single measurement. Advantages of using Equation 13 and Equation 14 are discussed below, including the ability to identify the extent of trapping and to identify when significant Förster-based aggregation occurs.

III. RESULTS AND DISCUSSIONS

To validate the utility of our intermediate solution to TTA, we next show that it provides an improved fit with better stability to both simulations and experimental data.

III.1. Kinetic Monte-Carlo Simulations

To test this model on a system of known conditions, we simulate exciton dynamics in an archetype phosphorescent OLED emissive-layer guest-host system using the open-source kinetic Monte-Carlo (kMC) simulation tool Excimontec[25–27]. Simulations are performed on a cubic grid of lattice points where each point is randomly assigned as either a guest or a host molecule. Triplet energies are chosen such that excitons are well confined on guest sites ($\Delta E_T = 0.4$ eV) and a variety of transport mechanisms, Gaussian energy disorders, and doping levels are chosen to test various scenarios. Details on the

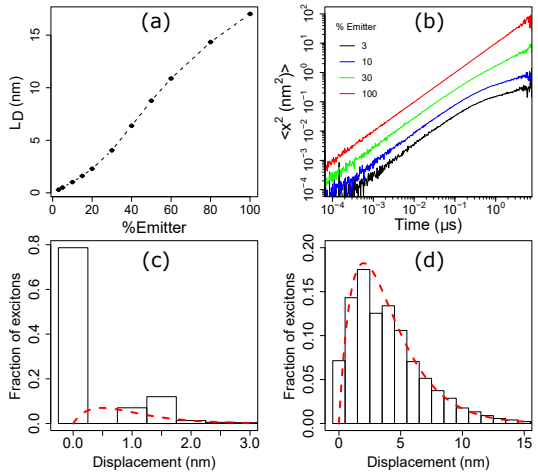

FIG. 1. (a) Diffusion length (L_D, calculated from root-mean-square displacements) dependence on emitter concentration. (b) The log-log plot of mean-square displacement vs. time, showing Fickian diffusion at high concentrations and differing diffusion regimes, for short and long times, at low emitter concentrations. Histograms of exciton root-mean-square displacements for (c) 3% emitter and (d) 30% emitter, both showing a significant population of trapped triplets with zero displacement.

simulations are given in the Experimental Methods section.

Figure 1 (a) shows an increase in exciton root-mean-square (RMS) displacements with increased guest concentration as more low-energy percolation paths are formed for the well-confined triplet excitons, as expected.

Figure 1 (b) show that at 3 *vol*% and 10 *vol*% emitter doping levels, which are of most interest in OLED application, the mean square displacement dependence on time has two different domains over the exciton lifetime: a Fickian diffusion regime at early times ($t \lesssim 300\ ns$) where $< x^2 > \propto t$, and an anomalous diffusion regime at time scales of the exciton lifetime ($t \gtrsim 300\ ns$) where $< x^2 > \propto t^a$, with $0 < a < 1$. KMC simulations show that even at 30 vol% guest, ∼7% of the excitons undergo zero displacement (Figure 1 (d)), whereas an analytical solution to the Fickian diffusion equation[28] (non-normalized fit to displacements > 5 nm) predicts precisely 0% will have zero displacement and ∼ 2.6% will have < 0.5 nm displacement. Therefore, the popular MSD diffusion model in Equation 5 is not strictly correct, as has been noted by multiple authors [16–18, 22, 29].

On the other hand, multiple authors have argued for using the SSF model described by Equation 11 to fit TRPL data for low guest doping levels where diffusion is limited [11]. However, contrary to the assumptions of the SSF model with no exciton diffusion, Figure 1 (c) shows that even at low guest concentrations (*e.g.*, 3 *vol*%), ∼ 20% of the excitons undergo diffusion. Consequently, the SSF model will not fully describe TTA process, even at these low doping levels. Hence, in the doping regime of interest to devices (*i.e.*, 5 to 12 *vol*%), we argue that the intermediate model (Equation 13) is more appropriate for fitting data.

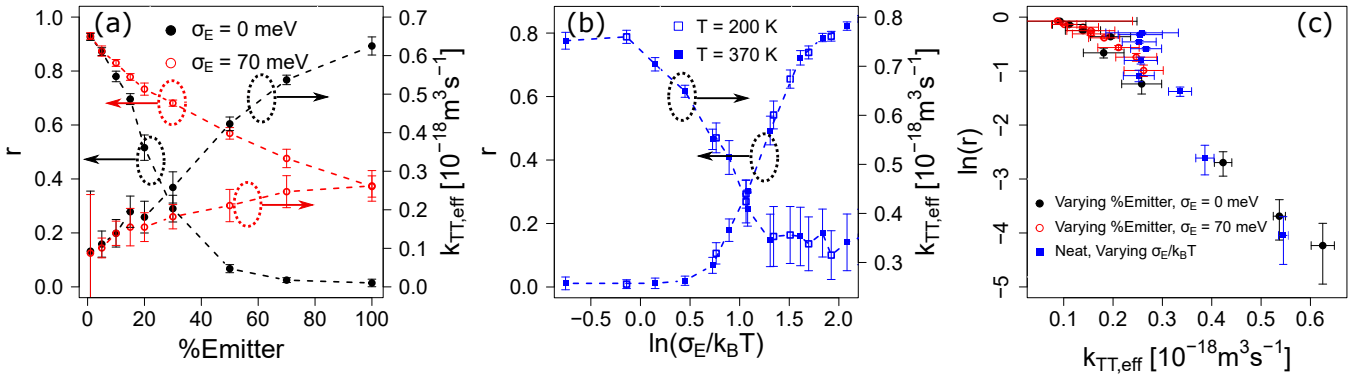

FIG. 2. Fit parameters r and $k_{TT,eff}$ in our intermediate model for (a) various emitter doping levels and either a flat or 70 meV Gaussian energy disorder at $T = 300$ K , (b) various Guassian energy disorder levels in a neat emitter, where σ_E is the standard deviation of a Gaussian distribution of triplet energy levels, k_B is the Boltzmann constant, and the model was tested at a system temperature of $T = 200$ K or $T = 370$ K, and (c) the correlation between r and $k_{TT,eff}$ for all data in (a) and (b).

The consistency of the fit parameter r, and its intuitive physical interpretation can be understood from its dependence on both spatial and Gaussian energetic disorder. Figure 2(a) shows that r is reduced as the doping level is increased, resulting from an increase in the number of low-energy (*i.e.*, guest) percolation paths and Figure 2(b) shows that an increase in Gaussian energy disorder in a neat film increases r. In both cases, as spatial or energetic disorder increases, so does the concentration of isolated, trapped excitons that are likely to decay radiatively without participating in TTA.Concurrently, an increase in guest doping level or decrease in energy dispersion increases exciton diffusivity due to guest detrapping[30], thereby increasing $k_{TT,eff}$, as shown in Figure 2 (a) and (b). Note that $k_{TT,eff}$ and r are inversely related in all

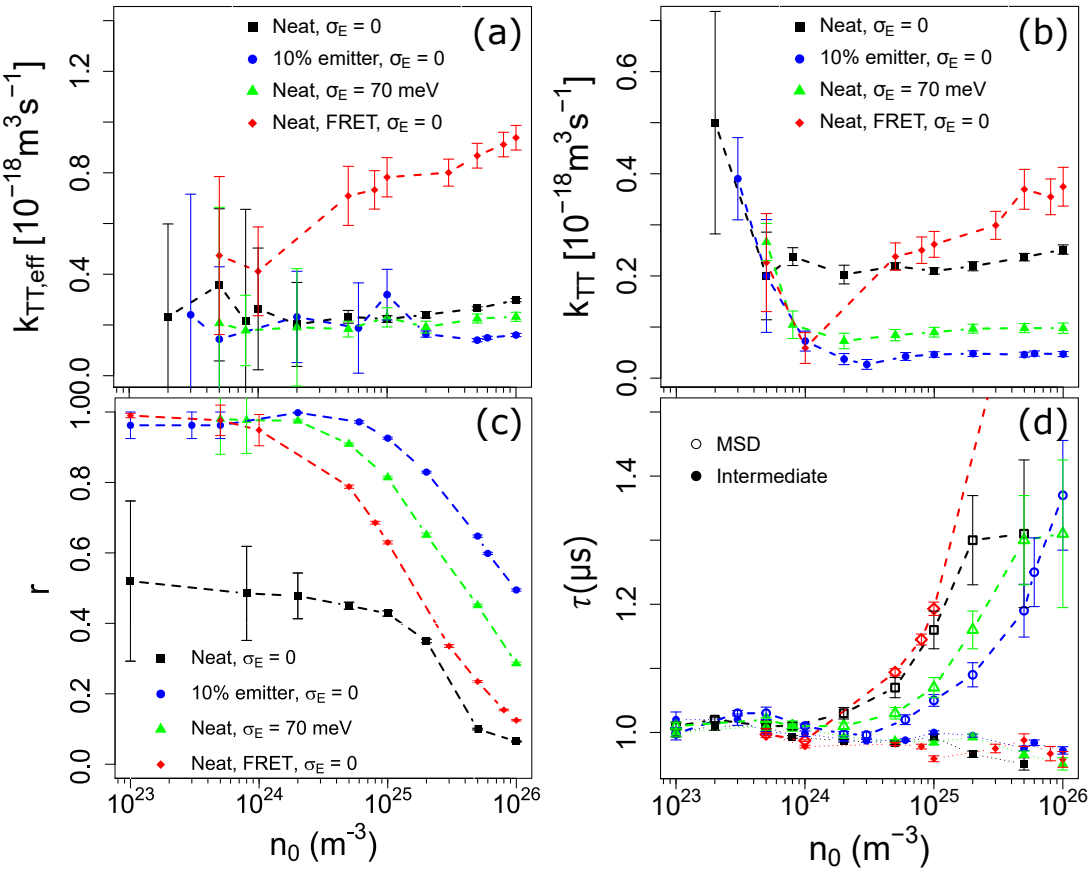

FIG. 3. (a) Fit parameter $k_{TT,eff}$ of the intermediate model vs. initial triplet concentration (n_0) for simulations with a MSD triplet-aggregation mechanism: for a neat material with no energy disorder, a 10 *vol*% guest sites with no energy disorder in a host matrix, and for a neat material with energetic disorder. The red curve is for simulations with FRET-mediated triplet aggregation. (b) The corresponding conventional k_{TT} values for the MSD model. (c) Fit parameter r of the intermediate model vs. n_0. (d) lifetime (τ) extracted with conventional MSD model (open symbols), and our intermediate model (closed symbols).

cases (Figure 2(c)).

III.1.1. Improved stability of k_{TT} rate fitting

A long standing issue is that the MSD model can not fit both the short- and long-lifetime regions of a TRPL curve and the value of k_{TT} obtained from fitting to MSD or SSF depends on the laser pulse excitation energy, time delays between the pulse and the beginning the fit, and the weighting method chosen [18]. Figure 3 (a) shows that $k_{TT,eff}$ in our intermediate model is independent of initial triplet populations in kMC simulations with Dexter-based aggregation for a neat film with flat energy landscape (black squares), 10 *vol*% randomly dispersed guest with no guest energy disorder (blue circles), and a neat system with Gaussian energetic disorder (green triangles). This improved fitting robustness relative to the MSD model, especially at low excitation levels (see sensetivity in Figure 3(b)), makes it significantly easier to compare results between different experiments and from different laboratories. Figure 3(c) shows that r decreases as n_0 increases for all simulation conditions. In all cases, as excitation density increases, the probability of a mobile exciton encountering a trapped exciton increases. Furthermore, we note that our intermediate model is better at extracting the actual radiative lifetime used in the simulations ($\tau = 1$ μs), especially at high excitation levels (see Figure 3(d)). However, $k_{TT,eff}$ extracted from simulations in which the triplet aggregation step is mediated by Förster transfer depend on the initial triplet population, as shown by the red curve in Figure 3(a). Therefore, the dependence of $k_{TT,eff}$ on excitation intensity can therefore be used to identify the dominant TTA mechanism in real systems using this intermediate model.

III.2. Experimental Results

Finally, we apply our intermediate TTA model to

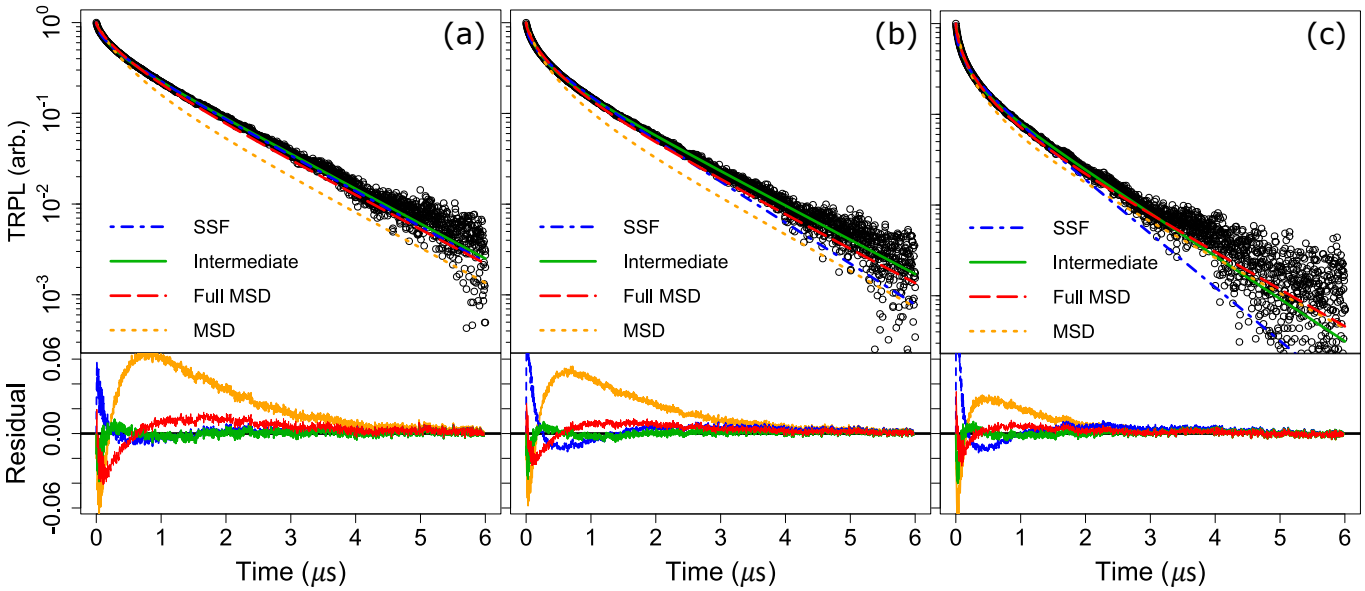

FIG. 4. Experimental TRPL data (black circles) for (a) 3 *vol*% $Ir(ppy)_3$:mCBP, (b) 10 *vol*% $Ir(ppy)_3$:mCBP, and (c) 30 *vol*% $Ir(ppy)_3$:mCBP, showing fits to our intermediate model (green), the single-step Förster model (blue), and the multi-step Dexter model from the general solution (red) and high diffusion approximation (orange). The lower panel of each graph shows the corresponding fit residuals.

***vol*%**	**Model**	$\mathbf{R_0}$ [nm]	**r**	τ [μs]	$\mathbf{k_{tt,eff}}$ [$10^{-18}\mathrm{m^3s^{-1}}$]
3%	SSF	2.66	—	1.11	—
	Intermediate	—	0.433	1.13	0.458
	Full MSD	—	—	1.15	0.086
	MSD	—	—	1.85	0.299
10%	SSF	3.07	—	0.96	—
	Intermediate	—	0.248	1.09	0.702
	Full MSD	—	—	1.15	0.182
	MSD	—	—	1.98	0.545
30%	SSF	3.63	—	0.73	—
	Intermediate	—	0.139	0.92	1.421
	Full MSD	—	—	1.06	0.435
	MSD	—	—	1.85	1.162

TABLE I. Fit parameters extract from experimental TRPL in Figure 4 using SSF model (Equation 11), intermediate model (Equation 13), Full-MSD (Equation 4), and MSD (Equation 6). $k_{TT,eff}$ values for the Full-MSD and MSD models correspond to k_{TT} of Equation 3 and $k_{TT,h}$ of Equation 6 respectively.

experimental TRPL data for conventional guest:host materials system with a high triplet-confinement energy, tris[2-phenylpyridinato-C2,N]iridium(III) ($Ir(ppy)_3$):3,3'-Di(9H-carbazol-9-yl)-1,1'-biphenyl (mCBP) ($\Delta E_T = 0.38\ eV$) [11, 31]. Because of the well localized exciton wavefunction in these organic materials and the large energy barrier ΔE_T that prevents triplets back-transfer onto host molecules, energy transfer between well-isolated guest molecules at low doping levels should follow the long-range SSF mechanism in Equation 11, while high guest concentrations allows formation of percolating low-energy diffusion paths, enabling MSD.

Figure 4 shows TRPL spectra for a 3 *vol*%, 10 *vol*% and 30 *vol*% $Ir(ppy)_3$ in mCBP and fit parameters corresponding to each model are reported in Table I. Below each TRPL spectrum are the corresponding residuals of the model fits, showing that the intermediate model has the smallest residual. Details of sample preparation and TRPL measurement are provided in the Experimental Methods section.

We employ the Akaike Information Criterion (AIC) to test the goodness of fit while penalizing additional fit parameters to the experimental data presented in Figure 4. Table II show that the intermediate model returns the lowest (best) AIC values ($\Delta_i \equiv 0$) for all guest concentrations tested, the SSF returns a middling positive Δ_i value and the MSD models perform the worst with the highest Δ_i value, especially for the 3 *vol*% and 10 *vol*% $Ir(ppy)_3$ concentrations. As expected, the AIC shows that the SSF model performs best at lower guest concentration and the MSD model improves as doping levels are increased.

Doping	**Intermediate**	**SSF**	**Full-MSD**	**MSD**
3 *vol*%	0	0.82	2.45	3.30
10 *vol*%	0	1.85	2.43	3.27
30 *vol*%	0	1.81	1.84	2.52

TABLE II. AIC values relative to that of the intermediate model (Δ_i), showing that the intermediate model has the best fit even when penalized against the additional fit parameters.

It can be seen that a fit to all terms in the MSD model results in the wrong lifetime in all three concen-

trations, which has significant impacts on the magnitude of the calculated k_{TT}, as has been pointed out in the literature[18]. The lifetime extracted from MSD is often so poor that people often fit the lifetime independently and fix it in their MSD fitting process. The intermediate model therefore significantly reduces differences in extracted $k_{TT,eff}$ for different excitation values, making it a more reliable and consistent estimator.

IV. EXPERIMENTAL METHODS

KMC simulations: Kinetic Monte Carlo simulations were performed using the open-source software, Excimontec [25, 32, 33]. All simulations use a $40 \times 40 \times 40$ cubic lattice with lattice constant a = 1 nm to simulate exciton transport and decay in a disordered host-guest system. The host-guest matrix is simulated by randomly assigning a fraction of the lattice sites to guest molecules and the rest to host molecules. Energetic disorder is simulated by randomly assigning each site a triplet energy E_T sampled from the Gaussian distribution $\exp\left(-E_T^2/2\sigma_E^2\right)/\sqrt{2\pi\sigma_E^2}$, where σ_E is the width of the distribution[34, 35]. Triplet exciton transport is simulated based on Miller-Abrahams rate[36, 37] and exciton quenching rates are based on Dexter model[9, 10], for the multi-step process, and Förster model [10, 38, 39], for the long range single-step process. In Table III we list important parameters used in the Excimontec simulations.

Parameter	Symbol	Value	Ref
Host	HOMO	6.0 eV	[40]
	LUMO	2.4 eV	[40]
Guest	HOMO	5.6 eV	[41, 42]
	LUMO	2.8 eV	[41, 42]
Triplet localization	γ	0.2 nm	[43, 44]
Förster radius	R_0	3.0 nm	[45]
Annihilation prefactor	R_{dex}	$10^{12}s^{-1}$	[45]
Hopping prefactor	ν_0	$10^{12}s^{-1}$	[15]

TABLE III. kMC simulation parameters.

Device fabrication: Materials for TRPL measurement were use as purchased from Luminescent Technology Corp (Lumtec). We deposited an 80 nm thick guest-host emissive layer by vacuum thermal evaporation onto quartz substrates at a background pressure of 1×10^{-6} Torr and ambient temperature. Samples were unloaded directly into a nitrogen-atmosphere glovebox and encapsulated with glass cover, using UV-vure epoxy, to prevent oxygen intrusion.

TRPL measurement details: TRPL measurements were performed on a in-house fabricated system consisting of a SRS NL100 nitrogen laser (337 nm wavelength, 170 μJ pulse energy), 400 nm long-pass filter, a photomultiplier tube (185-900 nm spectral response, gain$> 10^7$, 1.4 ns response time, Thorlabs PMTSS), a preamplifier (DC to 350 MHz, SRS SR445A), and a 100 MHz oscilloscope. Initial excitation densities are estimated to be $n_0 = 1.6 \times 10^{25}m^{-3}$.

V. CONCLUSIONS

In this work, we formulate an intermediate model (*e.g.* Equation 13) to better quantify triplet-triplet annihilation (TTA) process in real phosphorescent host-guest systems. This model is a first-order approximation using a weighed average of the high-diffusion-limit and pure radiative limit solutions to the TTA governing equation (Equation 2).

Our intermediate model has fit parameters r, which is a proxy for the portion of trapped excitons, and $k_{TT,eff}$ which lumps both Förster and Dexter based mechanisms into an effective TTA rate coefficient. We use kinetic Monte Carlo (kMC) simulations to verify the consistency and quality of the fit parameters and to demonstrate their intuitive physical interpretations. That is, the lifetime (τ) extracted with our intermediate model is consistent with the kMC simulation inputs and r increases as guest-doping levels are decreased and the site energy disorder is increased. The consistency of $k_{TT,eff}$ is demonstrated by its stability over different excitation densities, which will make comparing results from different laboratories easier. Furthermore, $k_{TT,eff}$ is nominally independent of energetic landscape in systems when Dexter-based aggregation is dominate, but when Förster -base aggreation is dominate, $k_{TT,eff}$ increases with pump intensity. The variation in $k_{TT,eff}$ at high pump intensity and the value of r at low pump intensity enable a way to differentiate between the effects of exciton trapping and SSF type mechanisms. Our intermediate model is then tested on experimental time-resolved photoluminescence measurements of a doping series in the $Ir(ppy)_3$:mCBP host-guest system and compared against the conventional multi-step Dexter (MSD) and single-step Förster (SSF) models. The Akaike Information Criterion (AIC) shows that the goodness of fit of our intermediate model is superior to that of the conventional MSD and SSF models.

VI. ACKNOWLEDGEMENT

Theory development and analysis was supported by the U.S. Department of Energy, Office of Science, Basic Energy Sciences under Award DE-SC0018021. Device fabrication, TRPL measurement capabilities, and our high performance computing node were funded by Universal Display Corporation. Funding sources had no involvement in this work.

[1] S. Reineke, K. Walzer, K. Leo, Triplet-exciton quenching in organic phosphorescent light-emitting diodes with Ir-based emitters, Physical Review B - Condensed Matter and Materials Physics 75 (2007) 1–13. doi:doi:10.1103/PhysRevB.75.125328.

[2] N. C. Giebink, S. R. Forrest, Quantum efficiency roll-off at high brightness in fluorescent and phosphorescent organic light emitting diodes, Physical Review B - Condensed Matter and Materials Physics 77 (2008) 1–9. doi:doi:10.1103/PhysRevB.77.235215.

[3] J. Saltiel, G. R. Marchand, W. K. Smothers, S. A. Stout, J. L. Charlton, Concerning the Spin-Statistical Factor in the Triplet-Triplet Annihilation of Anthracene Triplets, Journal of the American Chemical Society 103 (1981) 7159–7164. doi:doi:10.1021/ja00414a020.

[4] Y. Y. Cheng, T. Khoury, R. G. Clady, M. J. Tayebjee, N. J. Ekins-Daukes, M. J. Crossley, T. W. Schmidt, On the efficiency limit of triplet-triplet annihilation for photochemical upconversion, Physical Chemistry Chemical Physics 12 (2010) 66–71. doi:doi:10.1039/b913243k.

[5] X. Wang, R. Tom, X. Liu, D. N. Congreve, N. Marom, An energetics perspective on why there are so few triplet-triplet annihilation emitters, Journal of Materials Chemistry C 8 (2020) 10816–10824. doi:doi:10.1039/d0tc00044b.

[6] D. Y. Kondakov, W. C. Lenhart, W. F. Nichols, Operational degradation of organic light-emitting diodes: Mechanism and identification of chemical products, Journal of Applied Physics 101 (2007). doi:doi:10.1063/1.2430922.

[7] S. Scholz, D. Kondakov, B. Lüssem, K. Leo, Degradation mechanisms and reactions in organic light-emitting devices, Chemical Reviews 115 (2015) 8449–8503. doi:doi:10.1021/cr400704v.

[8] Y. Noguchi, H. J. Kim, R. Ishino, K. Goushi, C. Adachi, Y. Nakayama, H. Ishii, Charge carrier dynamics and degradation phenomena in organic light-emitting diodes doped by a thermally activated delayed fluorescence emitter, Organic Electronics 17 (2015) 184–191. URL: http://dx.doi.org/10.1016/j.orgel.2014.12.009. doi:doi:10.1016/j.orgel.2014.12.009.

[9] D. L. Dexter, A theory of sensitized luminescence in solids, The Journal of Chemical Physics 21 (1953) 836–850. doi:doi:10.1063/1.1699044.

[10] O. V. Mikhnenko, P. W. Blom, T. Q. Nguyen, Exciton diffusion in organic semiconductors, Energy and Environmental Science 8 (2015) 1867–1888. doi:doi:10.1039/c5ee00925a.

[11] A. Ligthart, X. de Vries, L. Zhang, M. C. Pols, P. A. Bobbert, H. van Eersel, R. Coehoorn, Effect of Triplet Confinement on Triplet–Triplet Annihilation in Organic Phosphorescent Host–Guest Systems, Advanced Functional Materials 28 (2018) 1–10. doi:doi:10.1002/adfm.201804618.

[12] D. G. Ha, J. J. Kim, M. A. Baldo, Link between hopping models and percolation scaling laws for charge transport in mixtures of small molecules, AIP Advances 6 (2016) 2–7. URL: http://dx.doi.org/10.1063/1.4948591. doi:doi:10.1063/1.4948591.

[13] H. Sirringhaus, 25th anniversary article: Organic field-effect transistors: The path beyond amorphous silicon, Advanced Materials 26 (2014) 1319–1335. doi:doi:10.1002/adma.201304346.

[14] Y. Zhang, S. R. Forrest, Triplet diffusion leads to triplet-triplet annihilation in organic phosphorescent emitters, Chemical Physics Letters 590 (2013) 106–110. URL: http://dx.doi.org/10.1016/j.cplett.2013.10.048. doi:doi:10.1016/j.cplett.2013.10.048.

[15] J. C. Ribierre, A. Ruseckas, K. Knights, S. V. Staton, N. Cumpstey, P. L. Burn, I. D. Samuel, Triplet exciton diffusion and phosphorescence quenching in iridium(III)-centered dendrimers, Physical Review Letters 100 (2008) 1–4. doi:doi:10.1103/PhysRevLett.100.017402.

[16] H. Van Eersel, P. A. Bobbert, R. Coehoorn, Kinetic Monte Carlo study of triplet-triplet annihilation in organic phosphorescent emitters, Journal of Applied Physics 117 (2015). doi:doi:10.1063/1.4914460.

[17] R. Coehoorn, P. A. Bobbert, H. Van Eersel, Effect of exciton diffusion on the triplet-triplet annihilation rate in organic semiconductor host-guest systems, Physical Review B 99 (2019) 1–10. doi:doi:10.1103/PhysRevB.99.024201.

[18] L. Zhang, H. Van Eersel, P. A. Bobbert, R. Coehoorn, Clarifying the mechanism of triplet-triplet annihilation in phosphorescent organic host-guest systems: A combined experimental and simulation study, Chemical Physics Letters 652 (2016) 142–147. doi:doi:10.1016/j.cplett.2016.04.043.

[19] L. Zhang, H. van Eersel, P. A. Bobbert, R. Coehoorn, Analysis of the phosphorescent dye concentration dependence of triplet-triplet annihilation in organic host-guest systems, Chemical Physics Letters 662 (2016) 221–227. URL: http://dx.doi.org/10.1016/j.cplett.2016.07.048. doi:doi:10.1016/j.cplett.2016.07.048.

[20] M. v. Smoluchowski, Versuch einer mathematischen theorie der koagulationskinetik kolloider lösungen, Zeitschrift fuer physikalische Chemie (Leipzig) 21 (1917) 98–104. doi:doi:10.1007/BF01427232.

[21] E. Engel, K. Leo, M. Hoffmann, Ultrafast relaxation and exciton-exciton annihilation in PTCDA thin films at high excitation densities, Chem. Phys. 325 (2006) 170–177. doi:doi:10.1016/j.chemphys.2005.09.004.

[22] M. Ansari-Rad, Transport and annihilation of the triplets in organic phosphorescent systems: Kinetic Monte Carlo simulation and modeling, J. Phys. Chem. C 125 (2021) 5760–5770. doi:doi:10.1021/acs.jpcc.0c10138.

[23] X. de Vries, R. Coehoorn, P. A. Bobbert, High energy acceptor states strongly enhance exciton transfer between metal organic phosphorescent dyes, Nature Communications 11 (2020) 1–8. URL: http://dx.doi.org/10.1038/s41467-020-15034-0. doi:doi:10.1038/s41467-020-15034-0.

[24] R. Coehoorn, P. A. Bobbert, H. Van Eersel, Förster-type triplet-polaron quenching in disordered organic semiconductors, Physical Review B 96 (2017) 1–11. doi:doi:10.1103/PhysRevB.96.184203.

[25] M. C. Heiber, A. Dhinojwala, Dynamic Monte Carlo modeling of exciton dissociation in organic donor-acceptor solar cells, Journal of Chemical Physics 137 (2012). doi:doi:10.1063/1.4731698.

[26] M. C. Heiber, A. Dhinojwala, Efficient Generation of Model Bulk Heterojunction Morphologies for Organic

Photovoltaic Device Modeling, Physical Review Applied 2 (2014). doi:doi:10.1103/PhysRevApplied.2.014008. arXiv:1407.4350.

[27] M. C. Heiber, A. Wagenpfahl, C. Deibel, Advances in modeling the physics of disordered organic electronic devices, Handbook of Organic Materials for Electronic and Photonic Devices (2019) 309–347. doi:doi:10.1016/b978-0-08-102284-9.00010-3.

[28] M. P. Silverman, Brownian Motion of Decaying Particles: Transition Probability, Computer Simulation, and First-Passage Times, Journal of Modern Physics 08 (2017) 1809–1849. doi:doi:10.4236/jmp.2017.811108.

[29] M. A. Baldo, C. Adachi, S. R. Forrest, Transient analysis of organic electrophosphorescence. II. Transient analysis of triplet-triplet annihilation, Phys. Rev. B - Condens. Matter Mater. Phys. 62 (2000) 10967–10977. doi:doi:10.1103/PhysRevB.62.10967.

[30] N. C. Giebink, Y. Sun, S. R. Forrest, Transient analysis of triplet exciton dynamics in amorphous organic semiconductor thin films, Organic Electronics 7 (2006) 375–386. doi:doi:10.1016/j.orgel.2006.04.007.

[31] S. A. Bagnich, A. Rudnick, P. Schroegel, P. Strohriegl, A. Köhler, Triplet energies and excimer formation in meta- and para-linked carbazolebiphenyl matrix materials, 2015. doi:doi:10.1098/rsta.2014.0446.

[32] A. F. Voter, Introduction To the Kinetic Monte Carlo Method, Radiation Effects in Solids (2007) 1–23. doi:doi:10.1007/978-1-4020-5295-8˙1.

[33] R. Coehoorn, H. Van Eersel, P. A. Bobbert, R. A. Janssen, Kinetic Monte Carlo Study of the Sensitivity of OLED Efficiency and Lifetime to Materials Parameters, Advanced Functional Materials 25 (2015) 2024–2037. doi:doi:10.1002/adfm.201402532.

[34] H. Bässler, Localized states and electronic transport in single component organic solids with diagonal disorder, Physica Status Solidi (B) 107 (1981) 9–54. doi:doi:10.1002/pssb.2221070102.

[35] R. Coehoorn, P. A. Bobbert, Effects of Gaussian disorder on charge carrier transport and recombination in organic semiconductors, Physica Status Solidi (A) Applications and Materials Science 209 (2012) 2354–2377. doi:doi:10.1002/pssa.201228387.

[36] A. Miller, E. Abrahams, Impurity conduction at low concentrations, Physical Review 120 (1960) 745–755. doi:doi:10.1103/PhysRev.120.745.

[37] A. Köhler, H. Bässler, What controls triplet exciton transfer in organic semiconductors?, Journal of Materials Chemistry 21 (2011) 4003–4011. doi:doi:10.1039/c0jm02886j.

[38] S. Sanderson, G. Vamvounis, A. E. Mark, P. L. Burn, R. D. White, B. W. Philippa, Unraveling exciton processes in Ir(ppy)3:CBP OLED films upon photoexcitation, Journal of Chemical Physics 154 (2021). URL: https://doi.org/10.1063/5.0044177. doi:doi:10.1063/5.0044177.

[39] A. Ruseckas, J. C. Ribierre, P. E. Shaw, S. V. Staton, P. L. Burn, I. D. Samuel, Singlet energy transfer and singlet-singlet annihilation in light-emitting blends of organic semiconductors, Applied Physics Letters 95 (2009) 2–4. doi:doi:10.1063/1.3253422.

[40] Y. Chen, X. Wei, Z. Li, Y. Liu, J. Liu, R. Wang, P. Wang, Y. Yamada-Takamura, Y. Wang, n-doping-induced efficient electron-injection for high efficiency inverted organic light-emitting diodes based on thermally activated delayed fluorescence emitter, J. Mater. Chem. C 5 (2017) 8400–8407. URL: http://dx.doi.org/10.1039/C7TC02406A. doi:doi:10.1039/C7TC02406A.

[41] C. Adachi, R. Kwong, S. R. Forrest, Efficient electrophosphorescence using a doped ambipolar conductive molecular organic thin film, Organic Electronics 2 (2001) 37–43. URL: https://www.sciencedirect.com/science/article/pii/S1566119901000106. doi:doi:https://doi.org/10.1016/S1566-1199(01)00010-6.

[42] Y. Q. Zhang, G. Y. Zhong, X. A. Cao, Concentration quenching of electroluminescence in neat ir(ppy)3 organic light-emitting diodes, Journal of Applied Physics 108 (2010) 083107. URL: https://doi.org/10.1063/1.3504599. doi:doi:10.1063/1.3504599. arXiv:https://doi.org/10.1063/1.3504599.

[43] M. Scheidler, B. Cleve, H. Bässler, P. Thomas, Monte Carlo simulation of bimolecular exciton annihilation in an energetically random hopping system, Chemical Physics Letters 225 (1994) 431–436. doi:doi:10.1016/0009-2614(94)87107-8.

[44] R. Saxena, T. Meier, S. Athanasopoulos, H. Bässler, A. Köhler, Kinetic Monte Carlo study of triplet-triplet annihilation in conjugated luminescent materials, Physical Review Applied 14 (2020) 1. URL: https://doi.org/10.1103/PhysRevApplied.14.034050. doi:doi:10.1103/PhysRevApplied.14.034050.

[45] J. R. Allen, A Study of Charge Transport : Correlated Energetic Disorder in Organic Semiconductors , and the Fragment Hamiltonian (2014).